Slow rupture of an aseismic fault in a seismogenic region of Central Italy

Antonella Amoruso,[1] Luca Crescentini,[2] Andrea Morelli,[3] and Roberto Scarpa[4]

Received 1 August 2002; revised 4 October 2002; accepted 11 November 2002; published 27 December 2002.

[1] Slow earthquakes and afterslips prove that the Earth does not have just two response time scales, i.e. that of tectonic loading and that of regular earthquakes. A swarm of slow earthquakes, with time constants of the order of hundreds of seconds, has been detected by a laser interferometer below the Gran Sasso massif (Italy). We analyse and model these observations to identify a very plausible source in a local fault, with no historic seismic behavior. While slow earthquakes occurring in subduction zones, and at the transition between locked and stably sliding segments of the San Andreas fault, are often associated with seismic events, in the case of the Apennines there is no correlation between local seismicity and slow earthquakes. Slow earthquakes, therefore, may also represent a specific failure behavior for a seismically locked fault, adding further complexity to the interpretation of geologic data for seismic hazard estimates. *INDEX TERMS:* 7209 Seismology: Earthquake dynamics and mechanics; 7223 Seismology: Seismic hazard assessment and prediction; 7230 Seismology: Seismicity and seismotectonics. **Citation:** Amoruso, A., L. Crescentini, A. Morelli, and R. Scarpa, Slow rupture of an aseismic fault in a seismogenic region of Central Italy, *Geophys. Res. Lett.*, *29*(24), 2219, doi:10.1029/2002GL016027, 2002.

1. Introduction

[2] Observations in Japan and California have proved the existence of faulting processes other than creeping (almost continuous slip without stress buildup) and regular earthquakes (sudden release of accumulated stress) [e.g., *Sacks et al.*, 1978; *Gladwin et al.*, 1994; *Kawasaki et al.*, 1995; *Linde et al.*, 1996]. These phenomena, known as slow earthquakes, have characteristic time scales ranging from tens of seconds to days, and release accumulated stress too slowly to produce seismic waves recordable by seismometers. They might play an important role in the stress redistribution process, and in reducing the seismic potential of active faults.

[3] Several clustered slow earthquakes have been observed from March to October 1997 [*Crescentini et al.*, 1999] by a geodetic interferometer located at 1400 m depth beneath the Gran Sasso massif (central Apennines, Italy) [*Crescentini et al.*, 1997]. The swarm was preceded by a few events since the end of 1996, and was followed by other episodic events in the next few months. Slow earthquakes appear as nearly-exponential strain changes (Figure 1) with duration from tens to thousands of seconds and amplitudes of a few nanostrains [*Crescentini et al.*, 1999]. Three additional slow earthquakes were recorded in May 2001.

[4] Until 1999 the interferometer measured difference in extension between one 90-m-long baseline oriented N66E and another 90-m-long baseline oriented N24W, i.e. one shear-strain component. Only since 1999 independent extensions of the two 90 m orthogonal baselines of the interferometer are measured, thus allowing areal strain to be also revealed. The shear-strain component of the 2001 signals is very similar to that of the 1997 events, and therefore presumably originate on the same fault. All the 2001 events give negative (compressive) or undetectable areal strain. No clear signal related to the slow strain events is detectable in the seismic records at the very-broadband seismographic station AQU, located about 17 km SW from the interferometer [*Boschi and Morelli*, 1994]. Lack of detection at AQU suggests a very local source.

[5] Here we consider these observations in an attempt to identify the source of the slow earthquake swarm. Although the information available can only be used to cast constraints on the location of the source, the conjunction of these constraints can nevertheless point to a very plausible candidate. Our favored fault, although known to geologists and mapped in neotectonic maps of the area, has no known seismic behavior.

2. Modeling and Comparisons

[6] The Gran Sasso massif is formed by carbonate sediments (dolomite and limestone above the study site) that overlie flysch and late-orogenic marine formations. It is located to the north-east boundary of a NW–SE oriented belt, 35–40 km wide, 100 km long, characterized by extensional faulting active from early Pleistocene up to the present [*Ghisetti and Vezzani*, 1999]. In the area surrounding the study site, the widely documented extensional regime is accommodated by two almost parallel systems of SW-dipping normal faults, approximately striking N95E to N110E. Faults are characterized by a thick unconsolitated gouge, probably saturated with water at hydrostatic pressure down to a few kilometers depth [*Ghisetti et al.*, 2001].

[7] Since full source inversion of available strain data is not possible, we have tested the possibility that the slow events occurred on a fault with strike 100°, dip 60°, and rake −90°, in agreement with the overall geological setup of the area.

[8] A seismic moment time history, compatible with the observed signals, is computed following a viscoplastic-

[1]Dipartimento di Fisica, Università dell'Aquila, L'Aquila, Italy, and Istituto Nazionale di Fisica Nucleare, Gruppo Collegato dell'Aquila, L'Aquila, Italy.
[2]Dipartimento di Scienze della Terra, Università di Camerino, Camerino, Italy, and Istituto Nazionale di Fisica Nucleare, Laboratori Nazionali del Gran Sasso, Assergi(AQ), Italy.
[3]Istituto Nazionale di Geofisica e Vulcanologia, Roma, Italy.
[4]Dipartimento di Fisica, Università di Salerno, Salerno, Italy.

0094-8276/02/2002GL016027$05.00

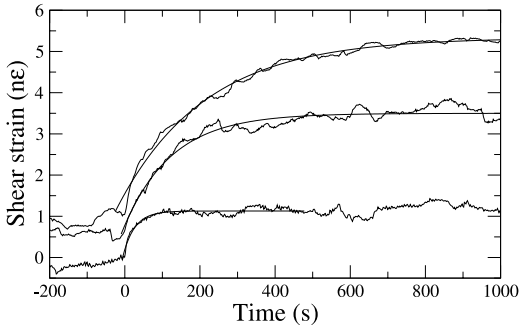

Figure 1. Three examples of recorded waveforms and best-fit exponentials. Amplitudes and rise times are 4.3×10^{-9} and 235 s, 2.3×10^{-9} and 128 s, 1.1×10^{-9} and 30 s from top to bottom.

gouge model for slow slip propagation [*Amoruso et al.*, 2002] and is nearly exponential in shape. Displacement of the monuments of the interferometer is computed for point sources in a flat layered Earth by using the AXITRA code [*Cotton and Coutant*, 1997]. Synthetic straingrams are obtained by difference between displacements. Sampling (0.5 Hz) and frequency content (up to the Nyquist frequency) have been chosen to match experimental data. Source depth is 4 km. The shape of the synthetic straingrams at the interferometer site for a given rise time mainly depends on the distance from the source (Figure 2) and, to a smaller extent, on fault angles and on source azimuth with respect to the interferometer. If distance is large, the far-field wavelet should be observed, but it is never visible in recorded signals. Several tests, made for different depths and positions of the source, indicate that the signals recorded by the interferometer have been generated by sources closer than approximately 10 km. Synthetic straingrams for these local sources are practically identical for

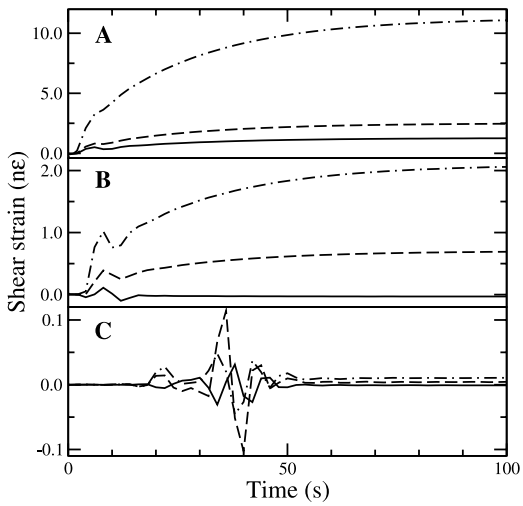

Figure 2. Synthetic signals at the interferometer site for point sources at different distances (A, 10 km; B, 20 km; C, 100 km) and azimuths (solid line, 90°; dashed line, 135°; dash-dotted line, 180°). Source parameters: depth 4 km, seismic moment 10^{15} Nm; rise time of the moment time history 30 s. A simple three-layer velocity profile (upper crust, lower crust, mantle) has been used.

various tested velocity profiles and for a homogeneous half-space.

[9] We have then computed the static response at the interferometer (both shear and areal strain) in case of a homogeneous elastic half-space (v_P = 5150 m/s, v_S = 2710 m/s, density = 2700 kg/m^3, rigidity = 2×10^{10} N/m^2) [*Okada*, 1992] moving the source on a 3D regular grid. Horizontal spacing is 100 m, over a square region 20×20 km^2 centered on the strainmeter. Vertical spacing is 1 km, from 1 to 7 km in depth. The number of observed events with positive sign is much higher (about 5 times) than the number of events with negative sign, and we record many more small-amplitude observed events than larger ones. Assuming that the sources of the slow events are clustered and located on a planar fault, the cluster has then to cross a surface of zero shear response and has to be located close to a surface of zero response in dilatation, in a small-gradient region. Only one source region, located few kms South of the interferometer, fully satisfies the constraints (Figure 3). Fault location and parameters are consistent with the well-known Vallefredda fault (fault 1 in Figure 4).

[10] We have also tested as possible sources all the faults, including minor ones, mapped on the neotectonic map in *Vezzani and Ghisetti* [1998] and located within approximately 10 km from the interferometer (Figure 4).

[11] The amplitudes of the recorded signals (and, therefore, of the seismic moment) scale with the square root of the rise time [*Crescentini et al.*, 1999]. We then multiply the amplitudes of the recorded signals by $10/\sqrt{\tau}$ (where τ is the rise time of each slow earthquake in seconds) to obtain normalized amplitudes for slow earthquakes with a reference τ = 100 s. We compare the normalized-amplitude frequency distribution of the observed events with the amplitude distribution computed for equal-sized rectangular sources regularly distributed on each of the seven fault

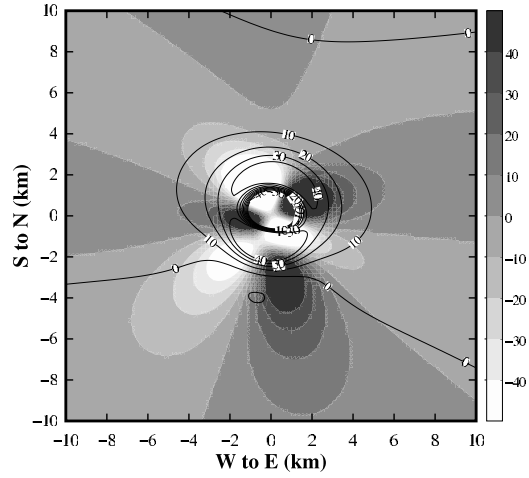

Figure 3. Shear (gray scale) and areal (contour lines) strain (in units of 10^{-9}) at the interferometer site for a point source (seismic moment 5×10^{14} Nm, dip 60°, rake −90°, strike 100°, depth 3 km) while varying its position around the interferometer. The only acceptable source region is located few kms South of the interferometer. The region located North of the interferometer must be rejected since the surface of zero areal strain dips toward North, i.e., in opposite direction with respect to the source.

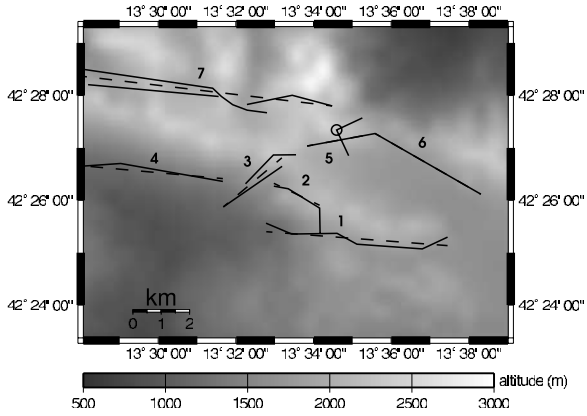

Figure 4. Map of the Gran Sasso region. Circle, location of the underground geodetic interferometer; solid lines starting from the circle, direction of the two interferometer arms; solid lines, surface trace of active faults [*Vezzani and Ghisetti*, 1998]; dashed lines, surface trace of tested planar faults.

planes, using the same Earth model as above. Observed and synthetic signals with normalized amplitude smaller than 1.2×10^{-9}, representing a conservative detection threshold, are discarded.

[12] For each of the faults, we compare the distribution of observed and synthetic amplitudes by means of the Kolmogorov-Smirnov test [*Press et al.*, 1992] which compares cumulative distributions of two data sets and computes the significance level P of the hypothesis that they are drawn from the same population, i. e. the significance of the similarity of the two distributions. The value of the seismic moment most appropriate for the sources of each tested fault is chosen by maximizing P. Several experiments have been performed, slightly moving and rotating each fault, testing different parts of it, and resizing rectangular sources. All the faults but number 1 strongly disagree with observations

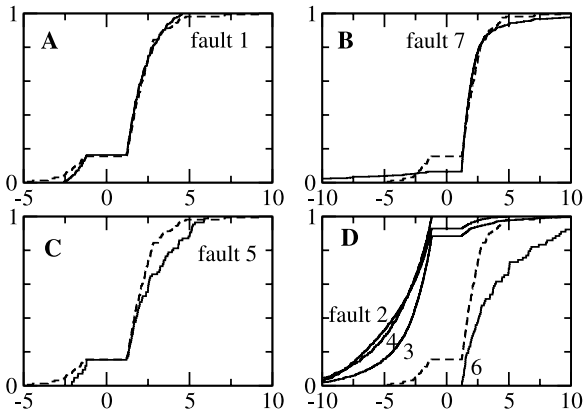

Figure 5. Cumulative distribution function (fraction of data points lower than a given value) versus amplitude of strain signals. Dashed lines in all plots represent the 161 observed normalized amplitudes larger than the threshold value. Solid lines represent synthetic signals from the different tested faults, after maximizing the significance level P. For faults in plot (D), retrieved P values are always zero and it is not possible to optimize parameters.

(Figure 5), while the agreement of fault 1 is extremely good, considering how crude the model is. The significance level P is 0.96 for fault 1, 0.28 for fault 7, less than 0.03 for fault 5 and practically zero for the other faults. Best significance levels for fault 1 are reached when slip distribution is confined to depths greater than about 2.2 km. The seismic moment for each point source, and consequently for an event with rise time $\tau = 100$ s, is 4.9×10^{13} Nm, and dimensions of the rectangular sources are 263 m along strike and 217 m along dip. Of all patches covering the slipped area, 196 produce signals above our detection threshold, in good agreement with the number (161) of observed signals having normalized amplitude above the threshold. Sources deeper than about 4.5 km (Figure 6) generate signals below the detection threshold, and we cannot exclude their existence. Additionally, sources on fault 1 give areal strain signals which are either detectable and compressive or undetectable, such as observed for the 2001 events.

[13] Due to the observed relation between amplitude A and rise time τ ($A \propto \sqrt{\tau}$), actual seismic moment for an event with rise time τ is about $4.9 \times 10^{12}\sqrt{\tau}$ Nm. A conservative estimate of the cumulative seismic moment of the 1997 swarm is about 1.9×10^{16} Nm, i. e. $M_W = 4.8$. This value is based on the assumption of absence of slip at depths greater than 4.5 km, and therefore represents a lower estimate.

[14] We have generated synthetic very-broadband seismograms for station AQU for different point sources on fault 1 and for different values of the rise time τ, using the same code as for monument diplacement. Seismograms have been obtained using the six-layer velocity profile of the global crustal model CRUST 5.1 [*Mooney et al.*, 1998], and several other models appropriate for the area. Although details of synthetic seismograms depend on the seismic velocity profile, they always appear undetectable in AQU records, in agreement with observations.

[15] The general picture given here is also somewhat supported by the occurrence of geochemical anomalies in the groundwater collected close to the interferometer [*Plastino and Bella*, 2001] during the same period [*Bella and Plastino*, 2000]. The pH increase from 8.0 to 8.3 is particularly noteworthy as it indicates rearrangement of

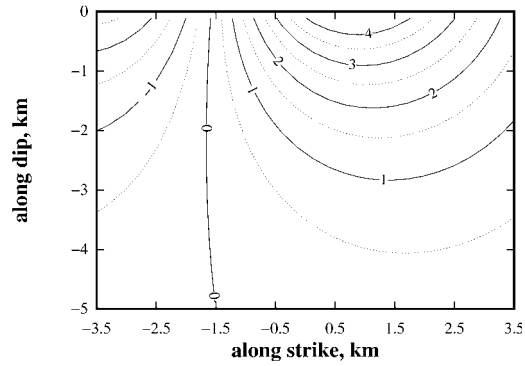

Figure 6. Amplitude (in units of 10^{-9}) of the synthetic signal at the interferometer site for a rectangular source (seismic moment 4.9×10^{13} Nm, side length 263 m along strike and 217 m along dip) while varying its position on fault 1. Upper side is at 2.2 km depth.

the flow of deep fluids, such as it would be caused by local deformation.

3. Conclusions

[16] Although the role of slow earthquakes in the seismogenic process is still an open question, they seem to play an important part in reducing stress accumulation in the Gran Sasso area, and consequently mitigating the potential for strong earthquakes. Small slow earthquakes (such as those discussed here) produce neither surface deformations detectable by GPS or other current geodetic technique, nor seismic waves that can be detected by usual seismometers or easily recognized in seismograms. This area does not show significant instrumental or historical records of seismicity. The activity we recorded probably originated on a fault which very likely did not exhibit seismic activity in historic times. This is a significant difference with respect to other reported slow ruptures where slow earthquakes have generally occurred on faults which also show seismic activity. These suggest the existence of different modes of rupturing of the same structure and that deformation developed through slow fracturing represents an intermediate mode between seismic activity and creeping [*Linde et al.*, 1996]. In our case evidence suggests that the fault is currently failing exclusively through slow fracturing. At least, it has done so during the sequence we documented.

[17] This fact may have important consequences on evaluating seismic hazard: a fault rated as active on geological grounds, may indeed be so. Yet its activity may be totally in the slow earthquake band, with no response in the seismic band of the spectrum. It is clear then that very-low frequency, high-sensitivity records of ground deformation contribute essential data to improve the real-time picture of seismic activity.

[18] **Acknowledgments.** We thank R. Basili, P. Bernard, and R. Gwyther for useful discussions and A. Bettini and E. Boschi for encouragement and support.

References

Amoruso, A., L. Crescentini, M. Dragoni, and A. Piombo, Fault slip controlled by gouge rheology: A model for slow earthquakes, paper presented at XXVII General Assembly of the European Geophysical Society, Nice, France, 2002.

Bella, F., and W. Plastino, LSS, Liquid Scintillation Spectrometry, Radon time series analysis at LNGS, I, *INFN-LNGS Annual Report 1999*, 193–198, 2000. (http://mercury.lngs.infn.it/lngs/report99/lss1.pdf)

Boschi, E., and A. Morelli, The MEDNET program, *Ann. Geofis. XXXVII*, 1066–1070, 1994.

Cotton, F., and O. Coutant, Dynamic stress variations due to shear faults in a plane layered medium, *Geophys. J. Int.*, *128*, 676–688, 1997.

Crescentini, L., A. Amoruso, G. Fiocco, and G. Visconti, Installation of a high-sensitivity laser strainmeter in a tunnel in central Italy, *Rev. Sci. Instrum.*, *68*, 3206–3210, 1997.

Crescentini, L., A. Amoruso, and R. Scarpa, Constraints on slow earthquake dynamics from a swarm in central Italy, *Science*, *286*, 2132–2134, 1999.

Ghisetti, F., and L. Vezzani, Depth and modes of Pliocene-Pleistocene crustal extension of the Apennines, (Italy), *Terra Nova*, *11*, 67–72, 1999.

Ghisetti, F., D. Kirschner, L. Vezzani, and F. Agosta, Stable isotope evidence for contrasting paleofluid circulation in thrust faults and normal faults of the Central Apennines, Italy, *J. Geophys. Res.*, *106*, 8811–8825, 2001.

Gladwin, M. T., R. L. Gwyther, R. H. G. Hart, and K. S. Breckenridge, Measurements of the strain field associated with episodic creep events on the San Andreas fault at San Juan Bautista California, *J. Geophys. Res.*, *99*, 4559–4565, 1994.

Kawasaki, I., Y. Asai, Y. Tamura, T. Sagiya, N. Mikami, Y. Okada, M. Sakata, and M. Kasahara, The 1992 Sanriku-Oki, Japan, ultra-slow earthquake, *J. Phys. Earth*, *43*, 105–116, 1995.

Linde, A. T., M. T. Gladwin, M. J. S. Johnston, R. L. Gwyther, and R. G. Bilham, A slow earthquake sequence on the San Andreas fault, *Nature*, *383*, 65–68, 1996.

Mooney, W. D., G. Laske, and T. G. Masters, CRUST 5.1: A global crustal model at 5 degrees × 5 degrees, *J. Geophys. Res.*, *103*, 727–747, 1998.

Okada, Y., Internal deformation due to shear and tensile faults in a half-space, *Bull. Seism. Soc. Am.*, *82*, 1018–1040, 1992.

Plastino, W., and F. Bella, Radon groundwater monitoring at underground laboratories of Gran Sasso (Italy), *Geophys. Res. Lett.*, *28*, 2675–2677, 2001.

Press, W. H., S. A. Teukolsky, W. T. Vetterling, B. P. Flannery, *Numerical Recipes in C, The Art of Scientific Computing, Second edition*, Cambridge Univ. Press, Cambridge, 1992.

Sacks, I. S., S. Suyehiro, A. T. Linde, and J. A. Snoke, Slow earthquakes and stress redistribution, *Nature*, *275*, 599–602, 1978.

Vezzani, L., F. Ghisetti, Carta geologica dell'Abruzzo, scale 1:100,000, *S.El.CA*, Firenze, 1998.

A. Amoruso, Dipartimento di Fisica, Università dell'Aquila, 67010 Coppito (AQ), Italy. (antonella.amoruso@aquila.infn.it)

L. Crescentini, Dipartimento di Scienze della Terra, Università di Camerino, 62032 Camerino, Italy. (luca.crescentini@unicam.it)

A. Morelli, Istituto Nazionale di Geofisica e Vulcanologia, Via di Vigna Murata 605, 00143 Roma, Italy. (morelli@ingv.it)

R. Scarpa, Dipartimento di Fisica, Università di Salerno, 84081 Baronissi (SA), Italy. (roberto.scarpa@sa.infn.it)